Mechanical and morphological variation of the human lumbar vertebral cortical and trabecular bone

Marcel E. Roy,[1] Jae-Young Rho,[1] Ting Y. Tsui,[2] Neal D. Evans,[3] George M. Pharr[2]
[1]*Department of Biomedical Engineering, University of Memphis, Memphis, Tennessee 38152*
[2]*Department of Materials Science, Rice University, Houston, Texas 77005*
[3]*Metals and Ceramics Division, Oak Ridge National Laboratory, Oak Ridge, Tennessee 37831*

Received 27 October 1997; accepted 27 July 1998

Abstract: The nanoindentation technique was used to characterize the variation in the elastic modulus and hardness of human lumbar vertebral cortical and trabecular bone. The elastic modulus (and in most cases, the hardness as well) of axially aligned trabeculae cut in the transverse direction was significantly greater than in other orientations of vertebral cortical and trabecular bone. In all cases, the elastic modulus and hardness of bone in the load-bearing direction was greater than in corresponding bone types cut in the other directions. Scanning electron micrographs of cortical shell revealed the Haversian-like canal systems expected in secondary cortical bone, but it was difficult to differentiate by morphology cortical from trabecular bone in the human lumbar vertebrae. © 1999 John Wiley & Sons, Inc. J Biomed Mater Res, 44, 191–197, 1999.

Key words: nanoindentation; elastic modulus; hardness; vertebral cortical shell; trabecular bone

INTRODUCTION

The microstructure, orientation, and anatomic location of bone are all important in determining its elastic properties.[1,2] It has been suggested that the Young's modulus of individual trabeculae (as opposed to bone structure) is less than that of cortical bone.[3,4] This difference may be explained by the presence of microstructural features, such as canaliculli, lacunae, and Haversian and Volkmann's canals, which become significant enough to affect the results of large-scale testing methods as specimen size decreases.[3] Bone anisotropy reflects the directionality in its microstructure and ultrastructure.[5] Kim and Walsh[6] measured the mechanical properties of a bovine femur in relation to position and orientation, discovering that the elastic modulus varied greatly with position along the long axis but did not vary in relation to its position radially or around the circumference. They concluded that positional variations may play an important role in the response of the bone to imposed loads.

Correspondence to: J.-Y. Rho; e-mail: jrho@cc.memphis.edu
Contract grant sponsor: Whitaker Foundation
Contract grant sponsor: Oak Ridge Institute for Science and Technology
Contract grant sponsor: U.S. Department of Energy; Contract grant numbers: DE-AC05-960R22464, DE-AC05-760R00033

© 1999 John Wiley & Sons, Inc. CCC 0021-9304/99/020191-07

Characterization of the structural elements of the vertebral body is important in understanding the mechanical behavior of the vertebral body as a whole. Mazess[7] suggested that the central trabeculae contribute only 30–50% of vertebral strength, with about 50–70% contributed by the cortical shell, endplates, and posterior elements. Silva et al.[8] also concluded that vertebral cortical shell may play an important role in vertebral fracture etiology. Moreover, the elastic properties of the cortical shell become more important with age.[9–11]

Nanoindentation methods emerged from hardness testing techniques as high-resolution load and depth-sensing instruments were developed. Hardness tests originally provided little more than a relative estimate of a material's resistance to penetration by a hard object.[12] Little information about a metal's or ceramic material's elastic properties could be gleaned from hardness tests until Doerner and Nix[13] published their nanoindentation method while studying the properties of thin films. However, their method assumed linear unloading and a flat punch indenter approximation. Oliver and Pharr[14] further improved the technique by characterizing the unloading process with a power law relation, using multiple loading and unloading cycles and a paraboloid indenter geometry. The primary advantage of the nanoindentation method is its ability to measure a material's properties on an extremely small scale. In a depth-sensing instru-

ment, hardness is measured continuously by recording the loads and displacements with high resolution as the indenter penetrates the surface of the material under test. A careful analysis of the load-displacement characteristics can provide not only hardness values but also yield information regarding elastic modulus.[14]

This study explores the variation of elastic modulus and hardness as functions of bone type (cortical vs. trabecular) and orientation within human lumbar vertebrae. If vertebral cortical and trabecular bone are significantly different materials, then their elastic properties should be significantly different. Vertebral bone morphology also was examined with a scanning electron microscope (SEM) to observe differences in lamellar morphology between cortical and trabecular bone.

MATERIALS AND METHODS

Three frozen L-1 vertebrae were obtained from human cadavers (one male, age 61, and two females, ages 57 and 66). After removing the processes, a 3 mm thick slice was cut out from the center of each vertebra body about its midsagittal plane [Fig. 1(a)] with a low-speed diamond saw lubricated with distilled water. The final piece obtained was most of the anterior/superior quadrant, about halfway down the anterior side and across the entire superior endplate [Fig. 1(b)]. After the marrow was removed with a distilled water jet, this piece was cut into three specimens for indentation in three different planes. The specimens were dehydrated in a series of alcohol baths, oriented, and embedded in epoxy resin. Dehydration artificially increases the measured modulus of bone, but it is necessary for the nanoindentation method and should not affect the relative differences between identically prepared specimens. The specimens were oriented such that sagittal, coronal, and/or transverse sections of the cortical endplate and shell could be indented, along with transverse and longitudinal sections of axial trabeculae, transverse and longitudinal sections of circumferential trabeculae, and longitudinal sections of radial trabeculae. Note that there were no indentations made in the radial transverse direction. Axial trabeculae run vertically and are aligned parallel to the axial skeleton. Circumferential and radial trabeculae both run horizontally, in the plane perpendicular to axial trabeculae, with circumferential trabeculae roughly concentric within the cortical shell and radial trabeculae roughly perpendicular to them. Because of the original midsagittal location of the specimen, it was relatively easy to distinguish between the two. However, the results ultimately would prove that data from longitudinal sections of both the circumferential and radial trabeculae could be lumped together without affecting the conclusions. The orientations obtained are listed in Table I along with the corresponding abbreviations.

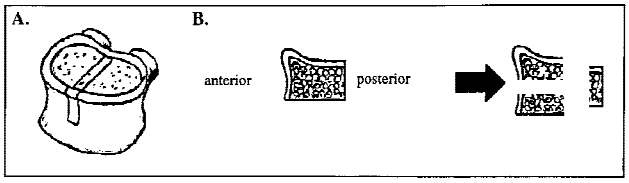

Figure 1. Sketches of (A) the origin of the sagittal slice cut from a vertebra body and (B) slice and secondary cuts (viewed from left side).

After allowing the embedded samples to cure, they were separated from their molds, cut to a uniform height, and metallographically polished to produce the smooth surfaces necessary for nanoindentation testing. Silicon carbide disks of decreasing abrasiveness (600, 800, and 1200 grit) first were used in succession, with final polishing by diamond suspensions (0.05 μm particle size). The 0.05 μm particle size was necessary to ensure that the final indentation depth of 1 μm was large relative to the surface roughness. Deionized water was used to lubricate the specimens during polishing and for subsequent rinsing between each polishing step.

Specimens were tested in a nanoindentation testing apparatus (Nano Indenter® II, Nano Instruments Inc., Knoxville, Tennessee) using a Berkovich diamond tip, which is characterized as a three-sided pyramid that makes an angle of 65.3° with the normal to the base. Thus the nanoindenters appear as equilateral triangles. Regions for indentation were selected with an optical microscope under computer control, acquiring five, ten, or twenty indentations in each specimen at each of the orientations listed in Table I. Although the elastic properties obtained from nanoindentation are primarily from the indentation direction, they also are influenced by properties in the transverse directions. However, this effect is not shown here. Before testing began, the indenter area function, or shape function, (that is, the cross-sectional area of the indenter as a function of the distance from its tip) was calibrated using a fused silica calibration standard. Fused silica is an ideal calibration standard because it is an isotropic solid.[14]

Before each indentation, the indenter was driven toward the specimen surface at a constant rate of 10 nm/s until surface contact was determined by the sudden increase in the stiffness of the delicate springs that support the center assembly to which the indenter is attached. The specimen surface was defined as that point where the stiffness reached a magnitude four times greater than the stiffness of the springs. After contact, the permanent hardness impression

TABLE I
Key to Orientation Abbreviations

Orientation	Source	Section
EC	Endplate	Coronal
ES	Endplate	Sagittal
SS	Cortical shell	Sagittal
ST	Cortical shell	Transverse
AL	Axial trabeculae	Longitudinal
AT	Axial trabeculae	Transverse
RL	Radial trabeculae	Longitudinal
CL	Circumferential trabeculae	Longitudinal
CT	Circumferential trabeculae	Transverse

Note that the properties of the RT (radial trabeculae, transverse section) orientation were not investigated in this study.

was made by driving the indenter into the specimen to a target depth of approximately 1 μm at a constant loading rate of 750 μ*N*/s until a total load of 8 m*N*, holding at this load for 10 s, and then unloading to 15% of the peak load at a rate equal to half that used during loading. At the end of the unloading cycle, the indenter was held on the surface for a period of 100 s to establish the rate of thermal drift in the machine and specimen for correction of the data, and then it was completely withdrawn. It should be noted that creep displacements were observed during the constant load hold period at peak load. This behavior could affect our results since the analysis procedures used to obtain mechanical properties from the nanoindentation load-displacement data are based on the notion that the upper portion of the unloading curve is dominated by elastic rather than plastic deformation. Thus, to minimize the effects of creep, a relatively long constant load hold period was inserted prior to the final unloading, during which the plastic deformation diminished to a negligible level.

Throughout this process, the indentation depth was monitored continuously as a function of load (see Figs. 2 and 3.) Although the loading segment is, in effect, a compression test, useful information is difficult to glean from it because the material undergoes plastic and elastic deformation simultaneously. The unloading data were curve fit according to power law relationships to determine the initial unloading slope, dP/dh. The elastic modulus then can be calculated from this slope, and the hardness can be determined using procedures described elsewhere.[14]

The indenter area function can be estimated by fitting the A versus h data to the relationship[14]

$$A = 24.5h^2 + C_1h + C_2h^{1/2} + C_3h^{1/4} + C_4h^{1/8} + C_5h^{1/16} + C_6h^{1/32} + C_7h^{1/64} + C_8h^{1/128} \quad (1)$$

where A is the indenter area function and h is the indentation depth. C_0 … C_8 are constants for the shape function determined during calibration. For a perfect tip, C_1 through C_8 are all equal to zero. A precise knowledge of the shape function of the indenter through careful calibration prior to testing and measurement of the plastic depth of contact is essential to the accuracy of this method because even a diamond indenter can become dull.

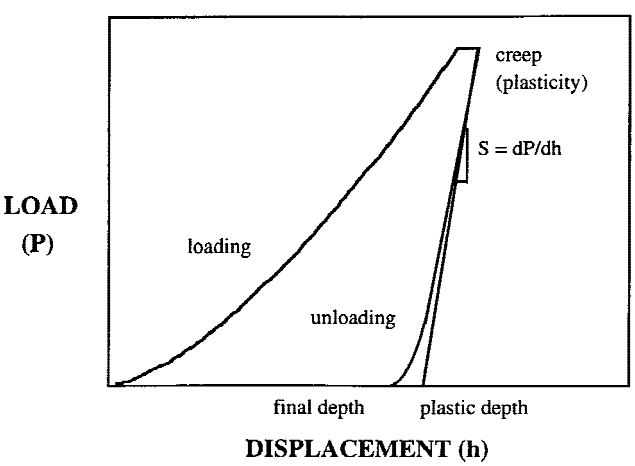

Figure 2. Sketch of a typical load-displacement curve from an indentation test.[14]

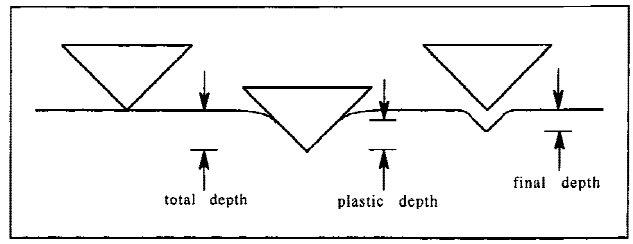

Figure 3. Schematic of the indentation process illustrating the decrease in indentation depth upon unloading.[13]

Given the area function at maximum load, the elastic modulus and hardness were calculated. Hardness (H), which physically represents the pressure that the material can support, is defined as the maximum load (P_{max}) divided by the area function (A):

$$H = \frac{P_{max}}{A} \quad (2)$$

Elastic modulus (E) is related to the contact stiffness (S), which is the measure of the resistance of a material to elastic deformation. As shown in Figure 2, contact stiffness (in force per unit depth) is measured from the load displacement data as the slope of the upper portion of the unloading curve and is related to the elastic modulus through:

$$E_b = \frac{1 - \nu_b^2}{\frac{2}{S}\sqrt{\frac{A}{\pi}} - \frac{1 - \nu_i^2}{E_i}} \quad (3)$$

where E and ν are the elastic modulus and Poisson's ratio, respectively, for bone (b) and indenter (i). For a diamond indenter, E_i = 1141 GPa and ν_i = 0.07, and the Poisson's ratio of bone was assumed to be 0.3. A sensitivity study has shown that varying ν_b in the range of 0.2 to 0.4 changed the measured values of E_b by no more than 8%.[15]

All scanning electron microscopy was performed with a Philips XL30 FEG (Philips Electronics N. V., Netherlands) after the specimens were indented. Charging effects in the SEM were reduced by carbon coating. Specimens were examined at an accelerating voltage of 10 keV. Backscattered (BSE) and secondary electron (SE) TIFF images were obtained at important locations on the bone specimens.

Significant differences in the elastic modulus and hardness were determined by one-way analysis of variance (ANOVA). When the analysis of variance revealed differences, Scheffé's test was employed (significance level: 5%) to test the hypothesis that there is a significant variation of Young's modulus and hardness as functions of differences in apparent bone material (cortical vs. trabecular) and orientation within human lumbar vertebrae.

RESULTS

Although the indenter head can be precisely targeted, after hundreds of indentations the error inherent in its positioning system adds up and can cause indentations to deviate slightly from their intended

targets. Because the indentation method is based on the solution to Boussinesq's problem, which assumes the material is a semi-infinite solid, indentations that end up too close to mechanical inhomogeneities (such as those that ended up too close to the bone/resin boundary or too close to microstructural features) were removed. After removing these unsatisfactory indentations from the data set, the elastic modulus and hardness in each orientation was determined (Table II). A statistical analysis revealed the orientations with significantly different elastic moduli and hardnesses (Table III).

Nanoindentation testing revealed axial trabeculae indented in the transverse direction exhibited the greatest value of the elastic modulus (and in two cases, the hardness as well), and they had significantly greater values than those of the other orientations, including the endplate and cortical shell. In every case, the elastic modulus of bone indented in the longitudinal (load-bearing) direction was greater than that of corresponding bone in the circumferential or transverse direction. Finally, the elastic modulus of horizontal transverse trabecular bone was significantly lower than that of the longitudinal endplate and the longitudinal shell.

Secondary and backscattered electron images were obtained from representative regions of each sample. Images presented illustrate the morphology of the endplate (Fig. 4); of the cortical shell (Fig. 5); and, for comparison, of ''true'' trabecular bone (Fig. 6).

DISCUSSION AND CONCLUSIONS

Nanoindentation is a relatively new technique that may provide an accurate and powerful tool for the analysis of intrinsic elastic properties of bone at the microstructural level. The nanoindentation method determines the intrinsic properties of bone on a scale smaller than microstructure but larger than ultrastructure. Unlike conventional micromechanical testing methods, where the effects of microstructural defects on data increase as the specimen size decreases, in nanoindentation the indentation site can be selected with precision to avoid microstructural defects altogether.[16] Nonetheless, this study was limited by the small sample size and the lack of normal physiological conditions in the testing procedure.

The nanoindentation method is only valid provided that the indentations are significantly deeper than the surface topography of the specimen and that the indentations are far away from defects. The indentation depth (1 μm) was used because the surface of the specimen was polished to a tolerance of 0.05 μm (or 50 nm). As one might expect, the scatter of elastic modulus and hardness data decreased as indentation depth increased.

Surprisingly, axial trabeculae indented in the transverse direction (AT) had the highest elastic modulus (22.7 GPa) and hardness (0.66 GPa) of the orientations

TABLE II
Summary of Nanoindentation Results

Orientation	No. Tests	Elastic Modulus (GPa) Mean	Elastic Modulus (GPa) SD	Hardness (GPa) Mean	Hardness (GPa) SD
EC	37	18.066	2.865	0.544	0.101
ES	48	16.668	2.864	0.536	0.100
SS	22	16.914	3.197	0.542	0.097
ST	36	18.059	2.663	0.549	0.073
AL	28	17.990	2.241	0.572	0.107
AT	14	22.715	3.124	0.664	0.098
RL	14	16.296	2.405	0.553	0.088
CL	15	15.679	1.466	0.553	0.063

TABLE III
Statistically Significant ($p < 0.05$) Results of Scheffé's Test (effect: orientation) for the Nanoindentation Data

Comparison	p values: Elastic Modulus (GPa)	p values: Hardness (GPa)
AT > EC	0.0003	0.0390
AT > ES	<0.0001	0.0116
AT > SS	<0.0001	0.0751*
AT > ST	0.0004	0.0629*
AT > AL	0.0006	0.3388*
AT > RL	<0.0001	0.2882*
AT > CL	<0.0001	0.2599*
AT > CT	0.0023	0.5632*

*Nonsignificant hardness differences.

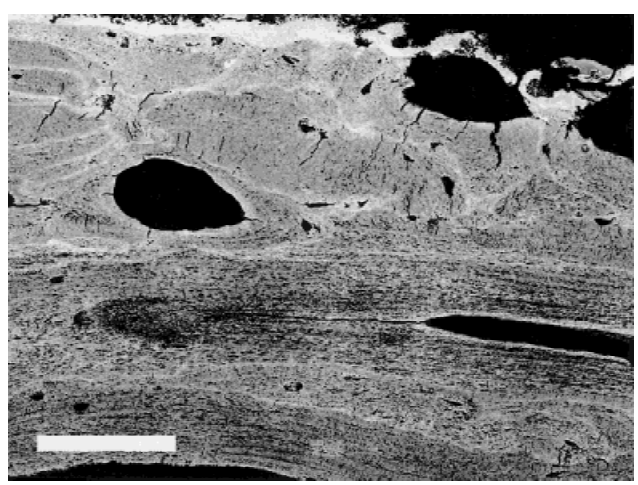

Figure 4. Backscattered scanning electron micrograph of the endplate, orientation ES (endplate, sagittal section). Note the thinning of the lamellar structure towards the bottom of the picture as it changes from cortical to true trabecular bone (top: outside of vertebral body; bottom: inside of vertebral body). Original magnification ×200. Bar represents 100 μm.

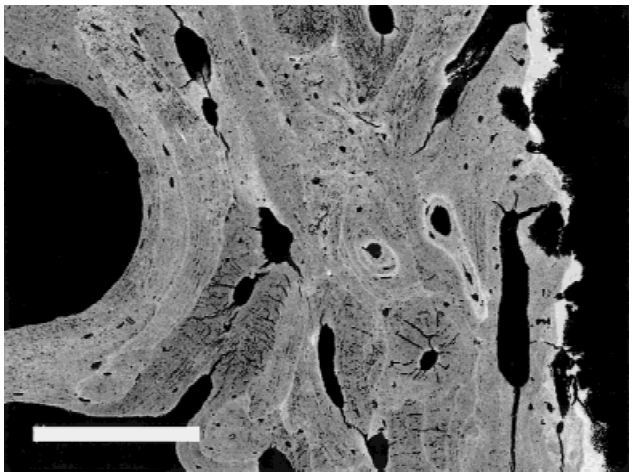

Figure 5. Backscattered scanning electron micrograph of cortical shell, orientation ST (cortical shell, transverse section). Note the seemingly chaotic morphology, the well developed lamellar structure, and the absence of well developed Haversian systems (left side: inside of vertebral body; right side: outside of vertebral body). Original magnification ×105. Bar represents 200 μm.

listed in Table II. As shown in Table III, this elastic modulus was significantly higher (significance level = 5%) than any other orientation, and the hardness was significantly higher than that of the endplate. The modulus is significantly higher than previously reported values for trabecular bone (4.87 GPa for longitudinal tibial specimens in bending).[3] Reilly and Burstein[17] reported an elastic modulus of 17.9 GPa for large, wet femoral cortical specimens in the longitudinal direction and 10.1 GPa in the transverse direction. Taking into account the increase in elastic modulus associated with the mechanical testing of dry bone,[18] the AT elastic moduli appear to be similar to those reported by Reilly and Burstein[17] for cortical bone in the longitudinal direction. However, this study found the elastic modulus of axial trabeculae indented in the longitudinal direction (AL) to be disproportionately higher at 18.0 GPa, such that the ratio of transverse to longitudinal elastic modulus is different (1.77 for Reilly and Burstein[17]compared to 1.26 in this study). Through nanoindentation of a porcine femur, Ko et al.[19] also observed an elastic modulus in trabecular bone (22 GPa) that was higher than their measurement of cortical bone (16 GPa). The nanoindentation measurements were each larger than corresponding microindentation values. However, they did not distinguish between the longitudinal and transverse directions. One would expect that the elastic modulus and hardness of bone would be highest in the load-bearing direction. This is held as a general rule, with statistical analysis revealing a significantly different magnitude only between AT and AL orientations of bone.

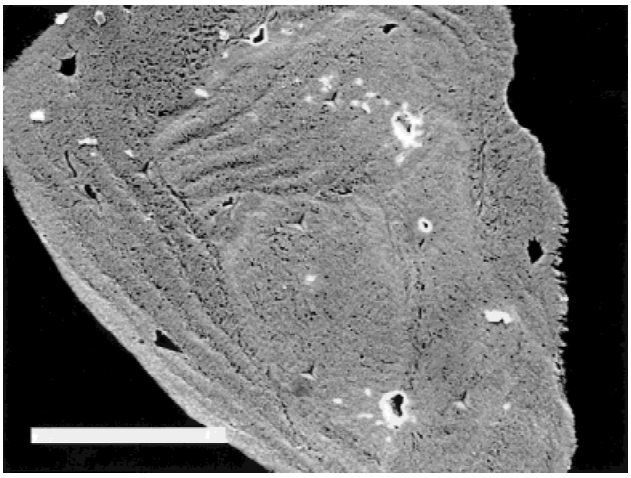

Figure 6. Scanning electron micrograph of a trabecular ''island'' of bone, orientation AT (axial trabeculae, transverse section). Five indentations are visible in the micrograph. Original magnification ×500. Bar represents 50 μm.

The results illustrate how the orientation and position affect the mechanical properties of human vertebrae. However, any conclusions should be arrived at carefully. In addition to being limited by the small sample size, the specimens were indented at various locations, so the variation of mineralization within the same specimen also could contribute to data scatter. However, for a biological material the standard deviation was relatively low.

Bone is often classified as ''cortical'' (less than 20% porosity) or ''trabecular'' (typically 50 to 90%). In addition, the presence of Haversian canal systems can be used as a defining characteristic of cortical bone. A typical vertebra is composed of a relatively thin and stiff cortical shell surrounding a less stiff trabecular core. Using a four-point bending test, Riemer et al.[4] found that the elastic modulus of human vertebral cortical bone is significantly larger than vertebral trabecular bone, suggesting a basic difference between the two types of bone. However, Silva et al.[8] recently concluded that the ''cortical'' shell of vertebra bodies may be a misnomer because of its porosity and thinness, and perhaps it would be better thought of as thin membranes of fused trabeculae rather than true cortices.

Several trends became apparent from the inspection of the SEM micrographs [Fig. 4 (ES), 5 (ST), 6 (AT)]. First, a highly calcified layer of connective tissue was found surrounding the ''cortical'' bone, which agrees with Boyde et al.[20] The outer layer of ''cortical'' bone seemed to be more chaotic and canal-filled, and the inner layer seemed to be less mineralized (darker in BSE images) and more lamellar (Fig. 4). The canals observed in the endplate tended to become more oval-shaped (as in Fig. 4) towards the endplate/shell junction, as if the canals were cut across at an oblique angle. This suggests that the canals are arranged in a spoke-like fashion in the endplate. The morphology present in Figures 4 and 5 echoes the view of Arnold,[21] who reported that the inner third of the cortical shell

is lamellar and the remainder Haversian. Finally, the relative structural density of the AT orientation is illustrated by comparing Figures 4 and 5 with Figure 6. This study could provide the foundation of a bone property ''mapping'' survey (for example, Nakabayashi et al.[22] and Sumner et al.[23]). However, the classifying parameters should be refined further. For example, the difference in degree of mineralization should be distinguished since mineral content affects the elastic properties of bone. In addition, nanoindentation was not performed anywhere near the endplate/shell junction. Its mechanical behavior at that transition and other areas may be interesting. The results also could be used in the development of further micromechanical models, such as supplying elastic properties for finite element modeling. Accurate finite element modeling of stress distribution in bone is limited by the accuracy of the parameters used as input. Previous analyses have used moduli for vertebral cortical shell ranging from 5.03 to 62.1 GPa.[24–28] The use of inaccurate input values in the modeling of the cortical shell and endplate could lead to a misinterpretation of the structural functions of vertebrae.

Overall, the nanoindentation data imply that the mechanical properties of vertebral bone generally are not significantly different as a function of bone type, aside from the unexpectedly high vertical longitudinal orientation of trabecular bone. This agrees with Silva et al.[8] as well as with the SEM micrograph conclusions. If cortical bone is defined as bone containing Haversian canal systems, then vertebral cortical bone is a misnomer. Although many canal systems were found (Fig. 5), the absence of lacunae in rings around the canals suggests that they may not be Haversian systems. The lack of distinction between the two types of bone was supported by the lamellar structure common to both the inner layers of ''cortical'' bone and the transverse trabecular bone of the same orientation. Thus it appears the differences between cortical and trabecular vertebral bone may be arbitrary.

This research was sponsored by the Whitaker Foundation and a junior faculty research fellowship from the Oak Ridge Institute for Science and Technology (JR). Analytical instrumentation for the nanoindentation testing was provided by the Division of Materials Sciences, U.S. Department of Energy, under contract DE-AC05-96OR22464 with Lockheed Martin Energy Research Corporation and through the SHaRE Program under contract DE-AC05-76OR00033 between the U.S. Department of Energy and Oak Ridge Associated Universities. One of the authors (GMP) is grateful for sabbatical support provided by the Oak Ridge National Laboratory.

References

1. Martin RB, Burr DB, editors. Mechanical Properties. In: The structure, function, and adaptation of compact bone., New York: Raven Press; 1989. p 57–84.
2. Mammone JF, Hudson SM. Micromechanics of bone strength and fracture. J Biomech 1993;26:439–446.
3. Choi K, Kuhn JL, Ciarelli MJ, Goldstein SA. The elastic moduli of human subchondral, trabecular, and cortical bone tissue and the size dependency of cortical bone modulus. J Biomech 1990; 23:1103–1113.
4. Riemer BA, Eadie JS, Wenzel TE, Weissman DE, Guo XE, Goldstein SA. Microstructure and material property variations in compact and trabecular vertebral bone tissue. Trans Orthop Res Soc 1995;20:529.
5. Turner CH, Chandran A, Pidaparti RMV. The anisotropy of osteonal bone and its ultrastructural implications. Bone 1995; 17:85–89.
6. Kim HD, Walsh WR. Mechanical and ultrasonic characterization of cortical bone. Biomimetics 1992;1:293–310.
7. Mazess RB. Fracture risk: A role for compact bone. Calcif Tissue Int 1990;47:191–193.
8. Silva MJ, Wang C, Keaveny TM, Hayes WC. Direct and computed tomography thickness measurements of the human lumbar vertebral shell and endplate. Bone 1994;15:409–414.
9. Mosekilde L, Mosekilde L. Normal vertebral body size and compressive strength: Relations to age and to vertebral and iliac trabecular bone compressive strength. Bone. 1986;7:207–212.
10. Buckwalter JA, Cooper RR. Bone structure and function. Instruc Course Lec 1987;36:27–48.
11. Faulkner KG, Cann CE, Hasegawa BH. Effect of bone distribution on vertebral strength: Assessment with patient-specific nonlinear finite element analysis. Radiology 1991;179:669–674.
12. Askeland DR, editor. Mechanical testing and properties. In: The science and engineering of materials. Boston: PWS Engineering Publishers; 1985. p 99–124.
13. Doerner MF, Nix WD. A method for determining the data from depth-sensing indentation instruments. J Mater Res 1986;1: 601–609.
14. Oliver WC, Pharr GM. An improved technique for determining hardness and elastic modulus using load and displacement-sensing indentation systems. J Mater Res 1992;7:1564–1583.
15. Rho JY, Tsui TY, Pharr GM. Elastic properties of human cortical and trabecular lamellar bone measured by nanoindentation. Biomaterials 1997;18:1325–1330.
16. Willems G, Celis JP, Lambrechts P, Braem M, Vanherle G. Hardness and Young's modulus determined by nanoindentation technique of filler particles off dental restorative materials compared with human enamel. J Biomed Mater Res 1993;27: 747–755.
17. Reilly DT, Burstein AH. The elastic and ultimate properties of compact bone tissue. J Biomech 1975;8:393–405.
18. Townsend PR, Rose RM. Buckling studies of single human trabeculae. J Biomech 1975;8:199–201.
19. Ko CC, Douglas WH, Cheng YS. Intrinsic mechanical competence of cortical and trabecular bone measured by nanoindentation and microindentation. Trans ASME: Bioeng Conf 1995; 29:415–416.
20. Boyde A, Jones SJ, Aerssens J, Dequeker J. Mineral density quantification of the human cortical iliac crest by backscattered electron image analysis: Variations with age, sex, and degree of osteoarthritis. Bone 1995;16:619–627.
21. Arnold JS. External and trabecular morphologic changes in lumbar vertebrae with aging. In: Progress in methods of bone mineral measurement. Washington, DC: U. S. Department of Health, Education and Welfare; 1970. p 352–411.
22. Nakabayashi Y, Wevers HW, Cooke TDV, Griffin M. Bone strength and histomorphometry of the distal femur. J Arthroplasty 1994;9:307–315.
23. Sumner DR, Willke TL, Berzins A, Turner TM. Distribution of

the Young's modulus in the cancellous bone of the proximal canine tibia. J. Biomech 1994;27:1095–1099.
24. Furlong DR, Palazotto AN. A finite element analysis of the influence of surgical herniation of the viscoelastic properties of the intervertebral disc. J. Biomech 1983;16:785–795.
25. Goel VK, Ramirez SA, Kong W, Gilbertson LG. Cancellous bone Young's modulus variation within the vertebral body of a ligamentous lumbar spine—Application of bone adaptive remodeling concepts. Trans ASME J Biomech Eng 1995;117:266–271.
26. Kurowski P, Kubo A. The relationship of degeneration of the intervertebral disc to mechanical loading conditions on lumbar vertebrae. Spine 1986;11:726–731.
27. Mizrahi J, Silva MJ, Keaveny TM, Edwards WT, Hayes WC. Finite-element stress analysis of the normal and osteoporotic lumbar vertebral body. Spine 1993;18:2088–2096.
28. Shirazi–Adl A, Drouin G. Nonlinear gross response analysis of a lumbar motion segment in combined sagittal loadings. J Biomech Eng 1988;110:216–222.